U. S. DEPARTMENT OF COMMERCE
NATIONAL OCEANIC AND ATMOSPHERIC ADMINISTRATION
NATIONAL WEATHER SERVICE
NATIONAL METEOROLOGICAL CENTER

OFFICE NOTE 172

A Partial Diagnostic Analysis of the 7L PE Output

Joseph P. Gerrity, Jr.
Development Division

FEBRUARY 1978

This is an unreviewed manuscript, primarily intended for informal exchange of information among NMC staff members.

1. Introduction

The '7L PE' model possesses several characteristics that distinguish it from its predecessor the '6L PE'. Most significantly, it provides more accurate forecasts. Technical differences appear in the forecast model and the postprocessing method.

Within the forecast model, the larger grid point array--129 x 129, (versus the previous 65 x 65), the smaller mesh size--190.5 km (versus 381 km), the use of a third stratospheric layer (versus the previous two stratospheric layers and a computational cap layer), the use of the upper boundary condition $\frac{dp}{dt} = 0$ at 50 mb (versus the previous $\frac{d\sigma}{dt} = 0$ at 0 mb), the use of a time-average of the pressure gradient, the stronger filtering of the temporal computational mode, the use of an explicit spatial diffusion term, and the use of a relatively longer time step constitute an impressive array of technical changes to the old model.

Within the postprocessing method, we find only two changes. The first change is associated with the existence of three rather than two stratospheric layers. The principal consequence of this change is the fact that the 100 mb level parameters are obtained by interpolation, rather than by extrapolation, of the forecast σ (sigma) coordinate variables.

The second postprocessing change is simply the extraction of "every other gridpoint" of the forecast model's array of 129 x 129 points to provide a 65 x 65 array on which the postprocessing is carried out.

With this as a background, I must stress the limited focus of the study presented in this note. The objective of this study was to assess the possibility that the "sampling" of the forecast variables, involved in the extraction of "every other point," might have led to an "aliasing" problem.

To show the potential for an 'aliasing' problem is fairly simple. Consider just one dimension and let the forecast variable F possess the Fourier series representation

$$F_\ell = \overline{F} + \sum_{n=1}^{64} [A_n \cos\frac{2\pi n\ell}{128} + B_n \sin\frac{2\pi n\ell}{128}] \tag{1}$$

on the 129 grid points with indices $\ell = 0, 1, \ldots, 128$. Similarly we may let $\hat{F}$ stand for the same forecast variable, 'sampled' at every other point of the 129 point grid. So

$$\hat{F}_k = F_{2k} \qquad k = 0, 1, \ldots, 64 \tag{2}$$

The sampled field may also be expressed by a Fourier series

$$\hat{F}_k = \tilde{F} + \sum_{n=1}^{32} [\tilde{A}_n \cos\frac{2\pi nk}{64} + \tilde{B}_n \sin\frac{2\pi nk}{64}] \tag{3}$$

on the 65 grid points with indices $k = 0, 1, \ldots, 64$. Using (1) and (2), one has

$$\hat{F}_k = F_{2k} = \overline{F} + \sum_{n=1}^{64} [A_n \cos\frac{2\pi nk}{64} + B_n \sin\frac{2\pi nk}{64}] \tag{4}$$

To relate (4) to (3), we observe that for $n > 32$, one may set $n = 64-\nu$ with ν a positive integer less than 32.

So (4) can be rewritten as

$$\hat{F}_k = \overline{F} + \sum_{n=1}^{31} [A_n \cos\frac{2\pi nk}{64} + B_n \sin\frac{2\pi nk}{64}]$$

$$+ A_{32} \cos\pi k + B_{32} \sin\pi k$$

$$+ \sum_{\nu=1}^{31} [A_{64-\nu} \cos\frac{2\pi\nu k}{64} - B_{64-\nu} \sin\frac{2\pi\nu k}{64}]$$

$$+ A_{64} \cos 2\pi k + B_{64} \sin 2\pi k \qquad (5)$$

Relating (5) and (4), one has

$$\left.\begin{aligned} \tilde{A}_n &= A_n + A_{64-n} \\ \tilde{B}_n &= B_n + B_{64-n} \end{aligned}\right\} \quad 1 \leq n \leq 31 \qquad (6)$$

$$\tilde{F} = \overline{F} + A_{64} \qquad (7)$$

$$\left.\begin{aligned} \tilde{A}_{32} &= A_{32} \\ \tilde{B}_{32} &= B_{32} \end{aligned}\right\} \qquad (8)$$

Defining $E_n^2 = A_n^2 + B_n^2$,

and $\hat{E}_n = \tilde{A}_n + \tilde{B}_n$, (9)

one has

$$\hat{E}_n^2 = E_n^2 + E_{64-n}^2, \qquad 1 \leq n \leq 31 \qquad (10)$$

It is the relationship (1) that underlies the 'aliasing' problem. Variability with high wave number ($n > 32$) on the full 129 point grid will appear to be low wave number ($n < 32$) in its sampled form, on the 65 point grid.

We must note however that the postprocessed variables (65 x 65 points) are subject to a digital filter, the H filter (cf. Office Note 169). The filter reduces the amplitude of the field $\hat{F}$ by a factor that depends on its wavenumber. With reference to equation (10), one has

$$\mathcal{E}_n^2 = R_H(n) \quad \hat{E}_n^2 = R_H(n)\left[\bar{E}_n^2 + E_{64-n}^2\right] \tag{11}$$

When one looks at the map of a completely postprocessed forecast variable, one is observing not the actual forecast, but a field with a structure modified by the sampling and filtering operation analytically expressed in equation (11). Naturally, one's curiosity is aroused. Are we seeing everything worthwhile, or are the "cosmetics" obscuring some intrinsic beauty? Are we being misled by the masquerade of the high wave numbers?

Now even within the narrow confines delineated above, our study is perforce further restricted by time and available resources. Allow me therefore to tell you what exactly I have done, what I have studied and what conclusions I have drawn.

Mr. Desmarais provided to me a set of σ coordinate variables ($\frac{\partial p}{\partial \sigma}$, θ and Z^*) produced as a 48 hour forecast by the 7L PE model. These data were for every 'fine mesh' gridpoint within the region shown in Figure 1. This region is 1/4 of the model's full domain and is covered by 65 x 65 'fine mesh' grid points.

I used this σ coordinate data and the postprocessing code 'SIGTOP' to obtain isobaric variables (T, Z) at each of the fine mesh points of the limited region. I used the 'GRDPRT' subroutine to print out the σ and isobaric data on the fine mesh grid and on a sampled set, 'every other point,' comprised of 33 x 33 points. I then used the IBM SSP subroutine FORIT to calculate the amplitude spectra of selected σ coordinate variables (θ_4, θ_5, P_σ (STRAT), P_σ (TROP), Z*), and of selected isobaric fields (Z and T at 850, 500, and 100 mb).

From the graphed spectra one may estimate the magnitude of the aliasing problem and from reconstruction of the fields with truncated versions of the Fourier series, one may estimate significance of energy in certain wave number bands. It seems that the 'aliasing problem' does not rise to a significant level, because the use of the H filter suppresses those waves to which 'aliased' energy makes a significant contribution. More tentatively I have an impression that some possibly significant wave-energy is being discarded by the current postprocessing scheme. This discarded energy has wave lengths between 6 and 8 fine mesh grid intervals (i.e. 1200 to 1600 km).

2. Horizontal Depiction of Data

I have available a large collection of output charts; the handful shown here concentrate upon the 100 mb level data. The other maps will be proferred to SEB for its consideration.

My first impression was that the stratospheric potential temperature fields were "noisy," whereas the tropospheric potential temperature and the $\frac{\partial p}{\partial \sigma}$ fields appeared relatively simple. When I constructed the "tropopause" pressure map (Figure 2) by re-isoplething the stratospheric $\frac{\partial p}{\partial \sigma}$ field, it became clear that the tropopause pressure was also relatively 'noisy.' Subsequently, I found that the postprocessed stratospheric, isobaric temperature fields were significantly less-noisy than the stratosphere σ-layer potential temperatures. From these observations I conclude that the very-noisy potential temperature field is associated in good measure to the large stratospheric static stability and the significant horizontal undulation of the pressure at the mid-point of the σ layers. This point will be raised again in my concluding remarks where I'll raise it in connection with the interpretation of $\dot{\sigma}$'s magnitude in the stratosphere.

In Figures 3A and 3B, the 100 mb temperature and height fields are shown for a portion of the fine mesh grid. The temperature isopleths are drawn at 5°K intervals; the height contours are drawn at 120 m intervals.

In Figures 4A and 4B, the same fields are presented at "every other gridpoint" of the domain shown in Figure 1. These are the 'sampled' fields.

In Figures 5A and 5B, one has the fields in the form that the operational postprocessor would produce them. The data in Figures 4 were subjected to the H filter to produce Figure 5.

One should note that the region shown in Figures 3 occupies the outlined section in the upper left of Figures 4 and 5. When Figures 3 and 5 are compared, the extent to which the postprocessor modified the 100 mb data stands out strongly.

In the next section I will show one dimensional spectra, calculated along rows 33, 35, ..., 51 of the fine mesh. These rows are "not uncharacteristically" noisy; indeed, the signal-to-noise ratio is larger for these rows than for rows 10, 12, ..., 28 which were also computed.

3. A Spectral View

In Figure 6 the spectra of the two $\frac{\partial p}{\partial \sigma}$ variables are shown together with the spectrum of the surface geopotential. These curves are called average spectra, because I first calculated the spectrum for each of 10 rows (every other row between 33 and 51) and then formed an average. They are normalized, because I divided each harmonic's amplitude by the amplitude of first harmonic. The amplitude of the first harmonic in appropriate units is shown in the legend.

We notice that the stratospheric $\frac{\partial p}{\partial \sigma}$ variable has larger relative amplitude than the other two variables over a broad range of harmonics (6 to 26). The amplitude of the tropospheric $\frac{\partial p}{\partial \sigma}$ first harmonic is greater than that of the stratospheric variable; this probably reflects the impact of the orographic variability.

Figure 7 shows the normalized average spectra for the potential temperature in σ layers 4 and 5. Layer 4 is the uppermost tropospheric layer, and layer 5 is the layer just above the troposphere. Since the

first harmonics have comparable amplitude, the much larger amplitude of θ_5's higher wave numbers is real. It is this feature that immediately impresses one, when the horizontal maps are examined. Note well, however, that the "energy" is distributed over a borad spectral band and has minimal content near the "two grid interval" wave (n = 32).

Although the σ layer data is not filtered (the postprocessed isobaric variables are), I have selected the spectrum of θ_5 to show the theoretical effects of sampling and filtering. In Figure 8, I show the un-normalized amplitudes of θ_5's harmonics between 0 and 16. The amplitudes of the higher harmonics have been "folded" back to produce the spectrum of the "sampled" data. Finally I show the result obtained when each of the sampled data's harmonics are reduced by the appropriate factor from the H filter.

It is clear that for the harmonics with Fourier index 6, or smaller, the sampling and filtering have minimal influence. The potential aliasing problem in the higher wave numbers is dominated by the action of the filter. We note however that the aliasing of energy into harmonics 7, 8, and 9 have the curious effect of leaving the "filtered" spectra with a "spectral bump" centered at harmonic 8. This particular harmonic has a wave length of four coarse-mesh grid intervals (8 fine mesh grid intervals). The question arises as to whether or not the spectral bump at harmonic 8 in the actual data is a realistic feature or is it a spurious feature. Currently operational methods "fortuitously" leave it relatively unmodified, rather than reducing its amplitude by the 0.75 factor that the H filter would yield!

I mentioned above that the signal to noise ratio is larger in the data on the rows 33 through 51 than at rows 10 through 28. Figure 9 documents this for the 100 mb temperature T and height Z. The four curves show the normalized average spectra for these variables. In the legend, the amplitudes of the first harmonics (the normalizing factor) are given. The "northern rows"* have more total variability as shown by the first harmonics; that is the signal is stronger in the northern rows. The "noise," harmonics with $n > 16$, has a larger ratio to the first harmonic by about a factor of two along the "southern" rows than along the "northern" rows. This fact may be attributable to the greater proximity of the lateral walls of the model to the "southern rows."

In Figure 10, we show that the postprocessed temperature fields possess considerably less noise than the σ coordinate potential temperatures (cp with Figure 7). In consequence of this fact, the aliasing problem is even less serious than it is with the σ variables. The figure also suggests that the mid-tropospheric temperature field (500 mb T) has less intermediate wave number ($8 \leq n \leq 13$) energy content than either the 850 or 100 mb levels. It is also evident that the noise level at 100 mb is about twice that at the other two levels.

To give a physical-space feeling for the implications of the spectral analysis, we may consider figures 11 and 12. Here we show the actual temperature at the fine-mesh gridpoints along row 41 which is near the middle of the set of "northern grid rows."

The relatively noise-free 850 and 500 mb temperatures are shown in Figure 11. The actual orography along this row is depicted along the base of the figure.

*Northern rows = 33, 35, ..., 51. Southern rows 10, 12, ..., 28.

It is interesting to notice the "bump" in the actual 850 mb temperature at gridpoint 13, and to observe the correlation with the orographic spike.

On this figure, I've plotted the 850 mb temperature reconstructed from the Fourier series coefficients for the first 6 harmonics (n = 6 included). This representation seems to be a nice expression for most of the field's actual variability. Yet it is clear that the minimum temperatures at grid points 13 and 22 are significantly under estimated by the truncated series. A wave structure between points 35 and 43 is also notably omitted by the truncated series. My intuition suggests that the truncated series is missing details of some real predictive value.

Now we turn to the last illustration, Figure 12. There the actual 100 mb temperature is shown at each grid point of row 41. First we notice that this field is negatively correlated with the tropospheric temperatures, as it should be. Then we may note that the jagged spikes of the actual field, have amplitudes of less than 3 degrees and are not dominant. They also display very little of the "lattice separation" characteristics of unstable numerical solutions.

Two other curves are shown on the figure. These depict the temperatures reconstructed from the Fourier series coefficients truncated at the 6th and 11th harmonics respectively. While the reader is free to judge for his (her) -self, it is my opinion that the 11 mode representation is not a "better" representation of the 100 mb temperature field.

So, it seems to me that the spectral information content of the temperature field is confined to relatively longer wave lengths in the stratosphere (100 mb) than in the troposphere (850, 500 mb). Perhaps the postprocessor should account for this fact!?

4. Concluding Remarks

This study proved interesting to me, but the computer readily yields so much data that the time required to thoroughly assimilate the information tends to stretch beyond the bounds available to the casual investigator. For this reason, I hope that this note may stimulate a more far reaching investigation along the lines pursued here and on other courses.

Earlier I promised to conclude with a comment on the noisy character of the stratospheric potential temperature field. I have just two observations:

(1) The adiabatic vertical motions

$$\omega_A \simeq -\frac{1}{S}\vec{V}\cdot\nabla\theta$$

are probably "horrendous" complicated, do they have value?

(2) If the stratosphere is so noisy and really only has "6 information bearing harmonics" wouldn't a spectral model do a better job for the stratosphere?

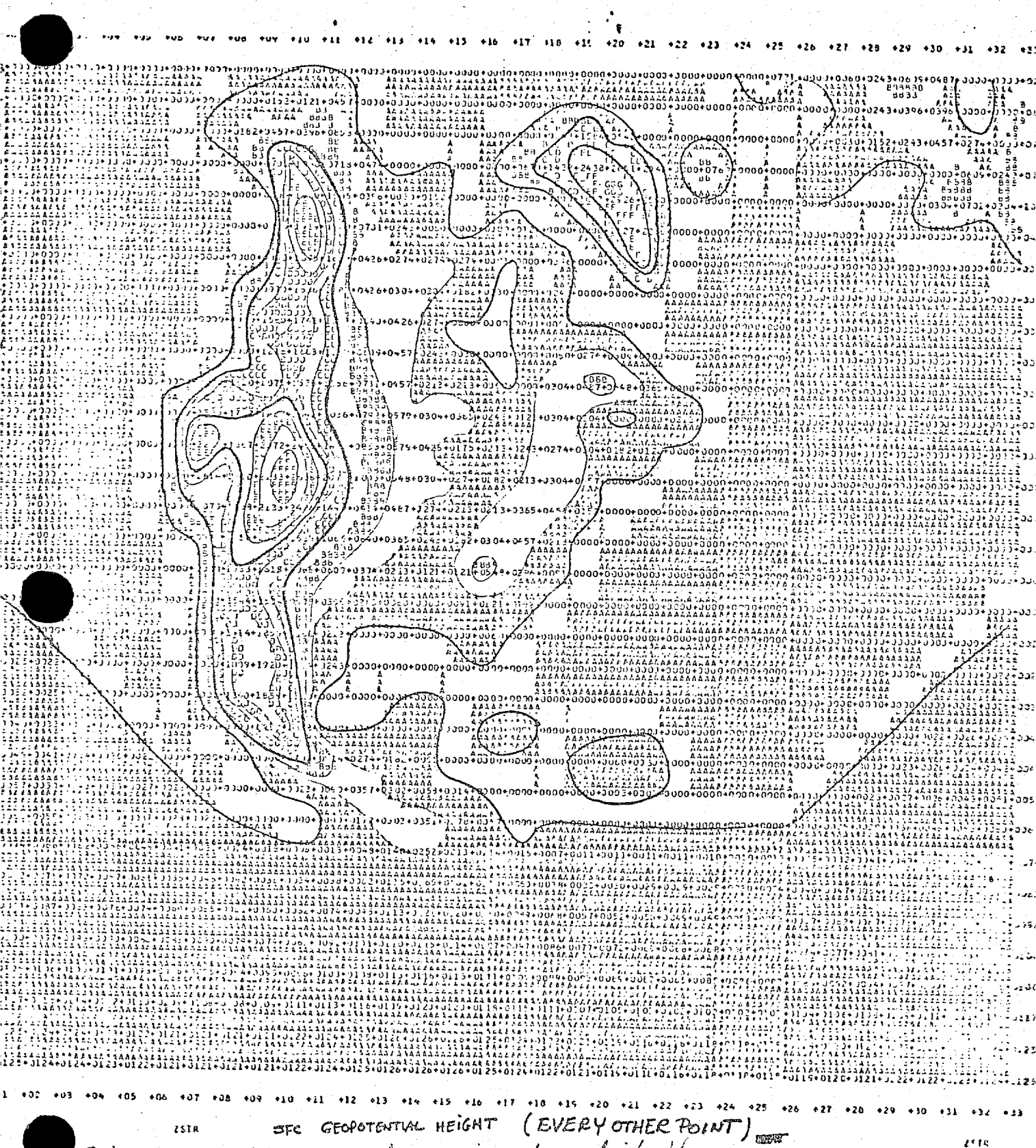

ZSTR 3FC GEOPOTENTIAL HEIGHT (EVERY OTHER POINT)

Figure 1. Showing the region for which the model's forecast was available.

ISOPLETHS OF "TROPOPAUSE" PRESSURE (EVERY OTHER POINT)

figure (2)

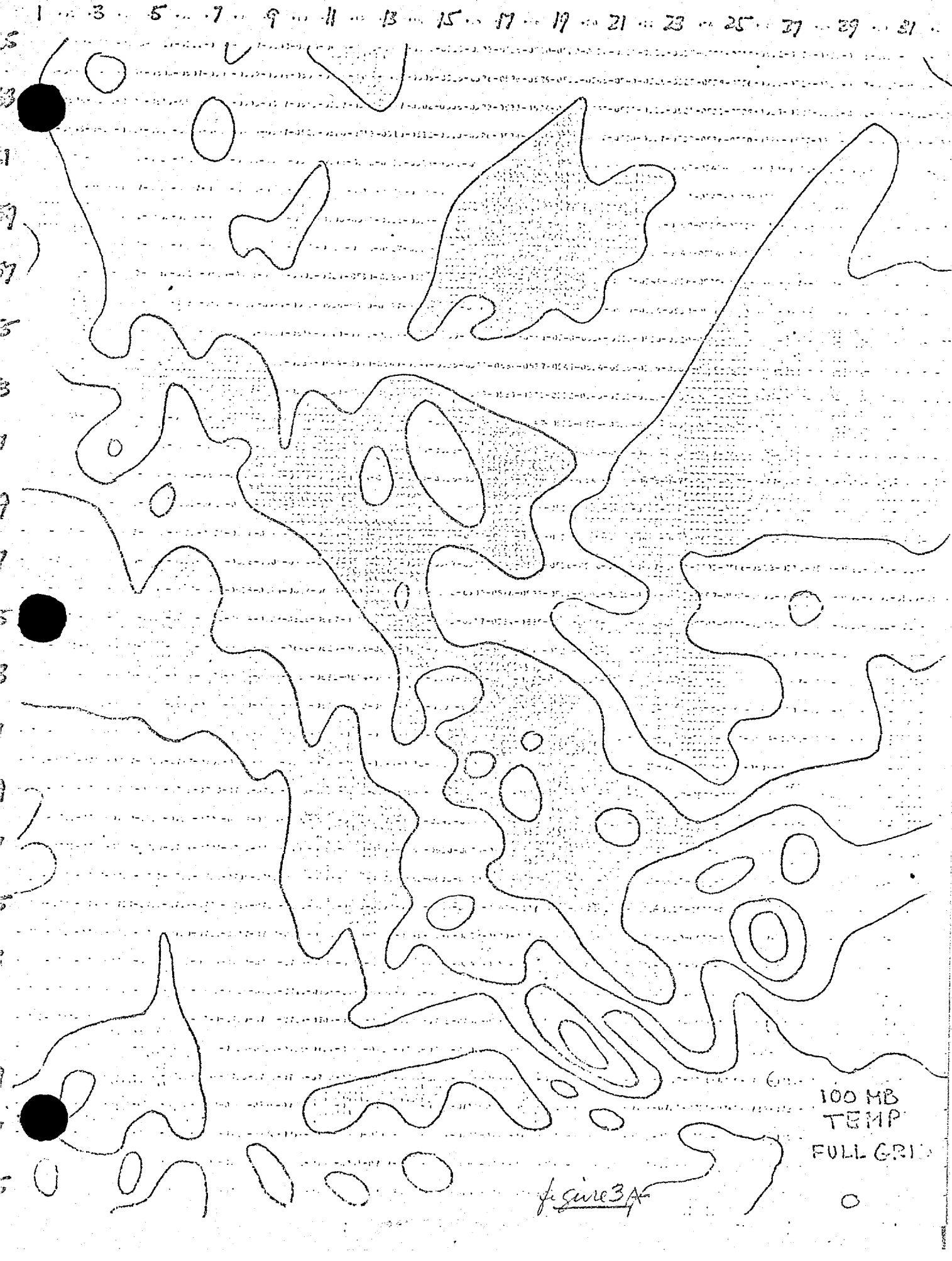

figure 3A

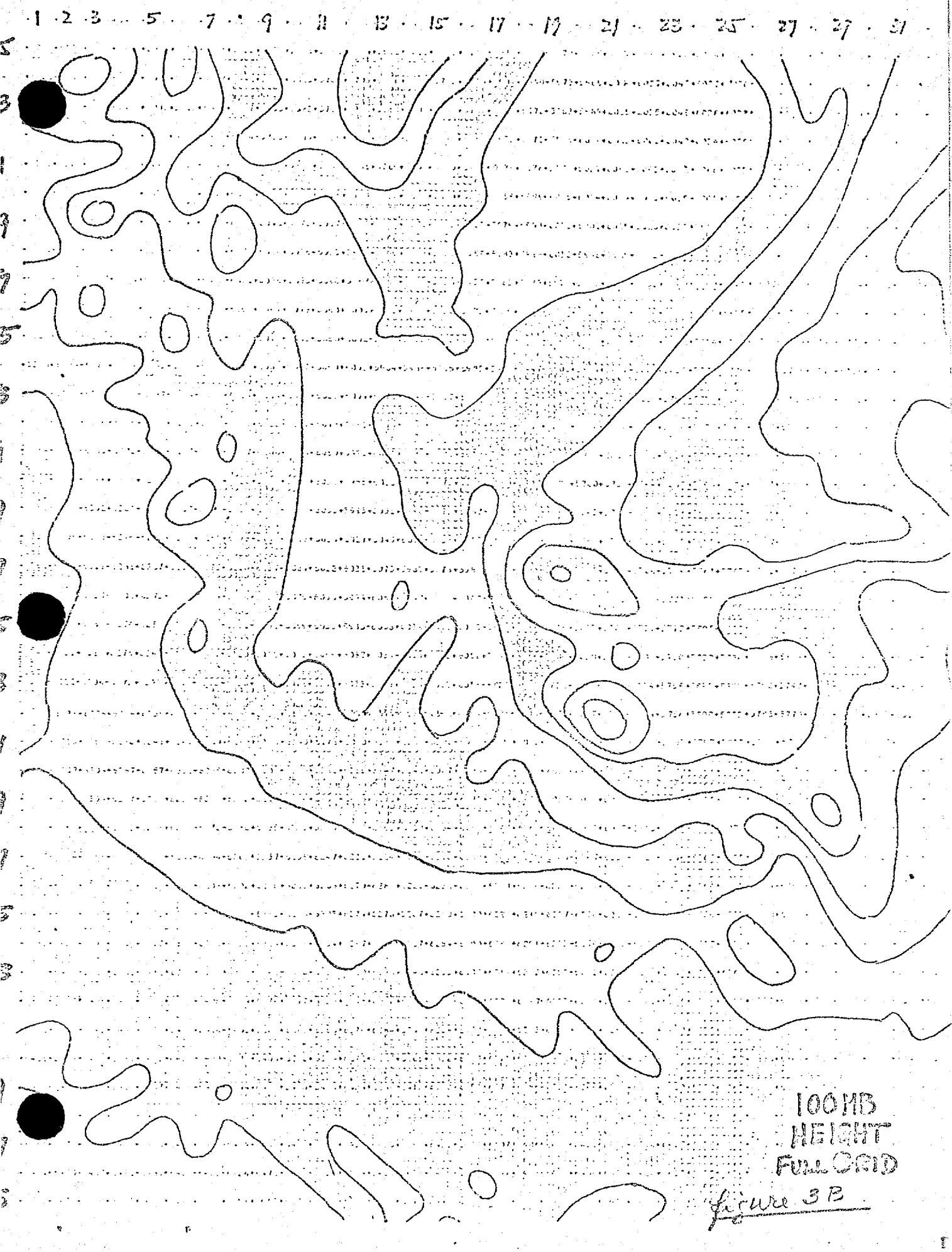

figure 3B

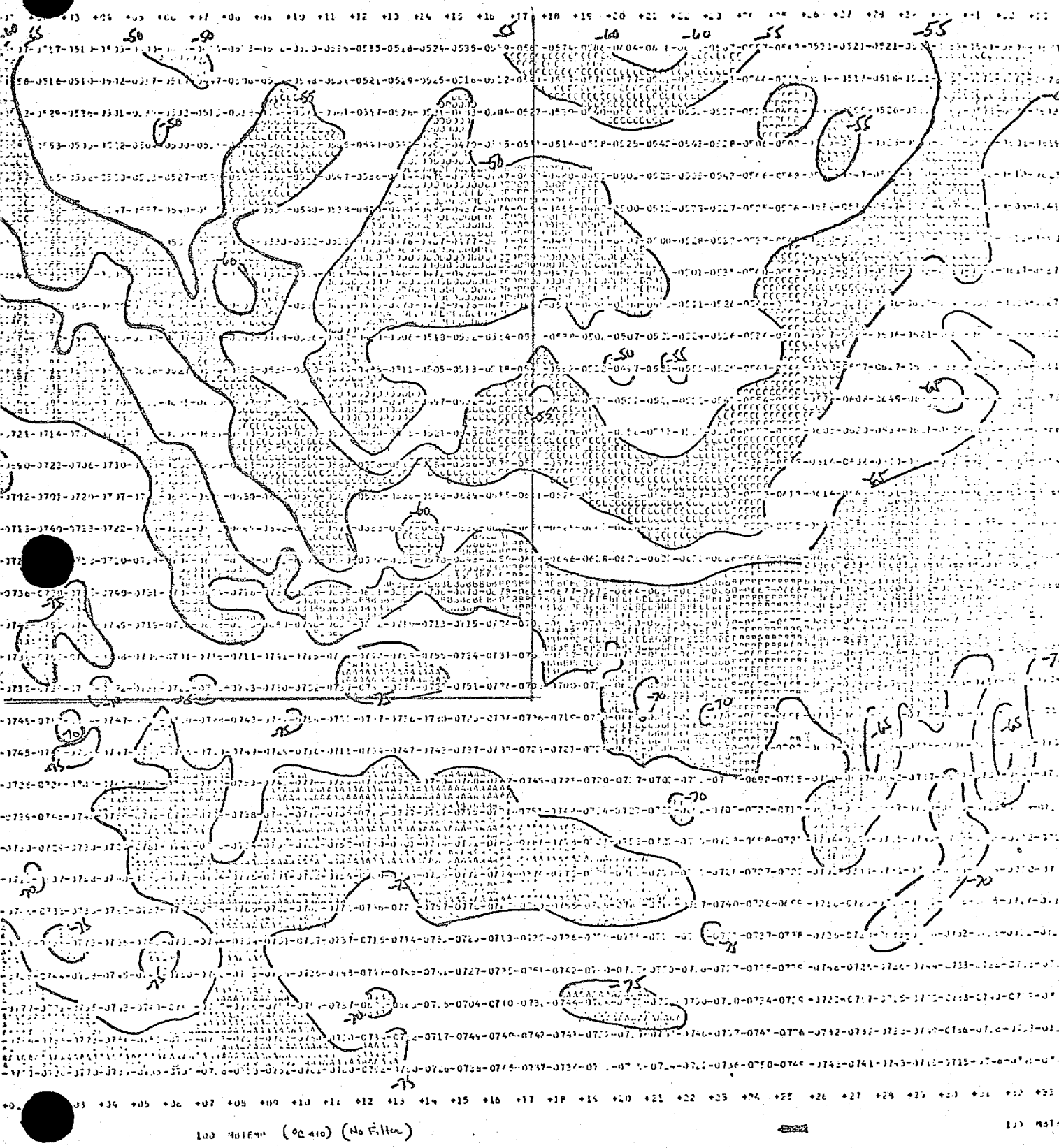

(OC 410) (No Filter)

figure 4A

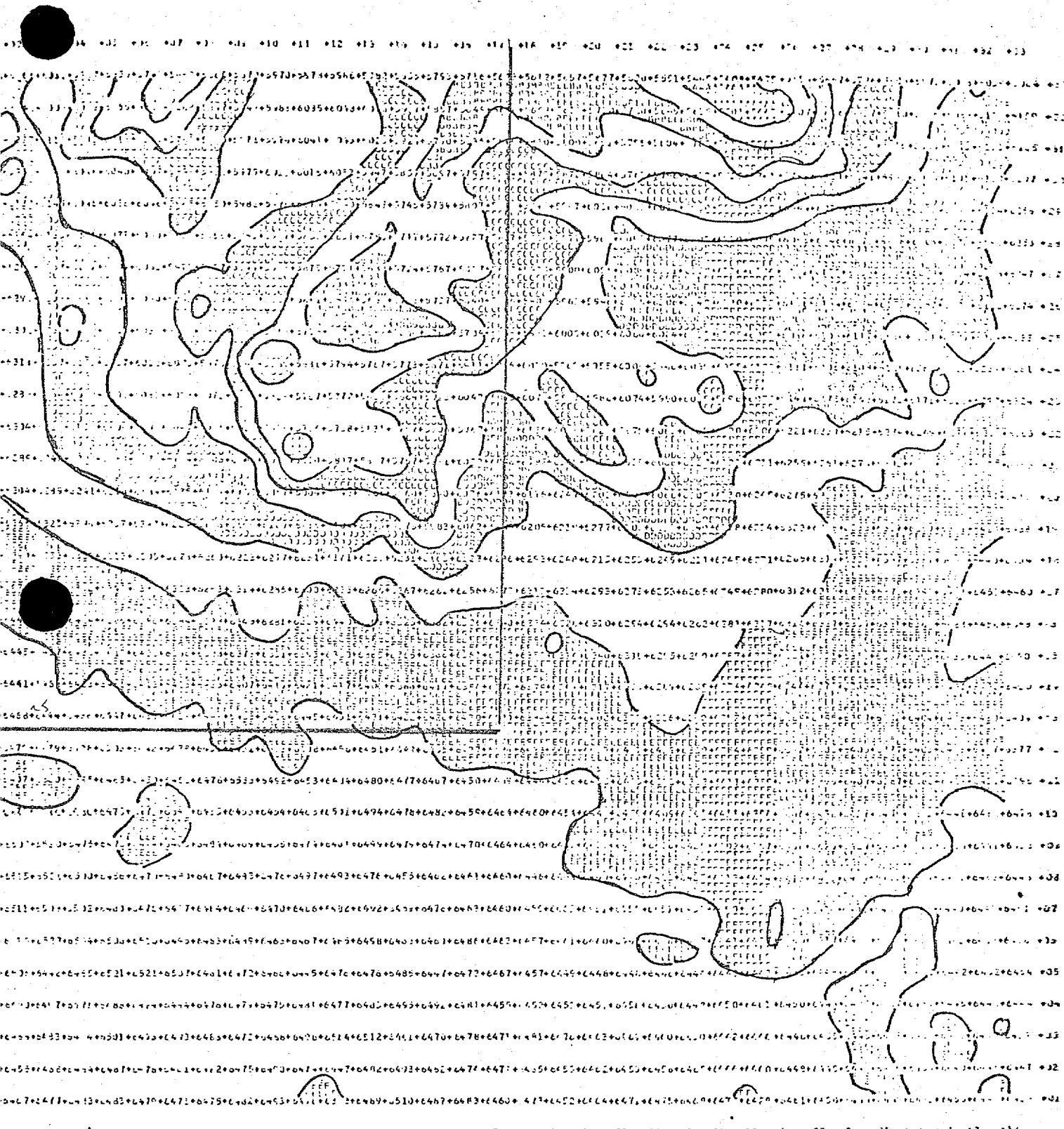

100 MB GEOPOTENTIAL HEIGHT (LESS 10km) (NO FILTER)

figure 4B

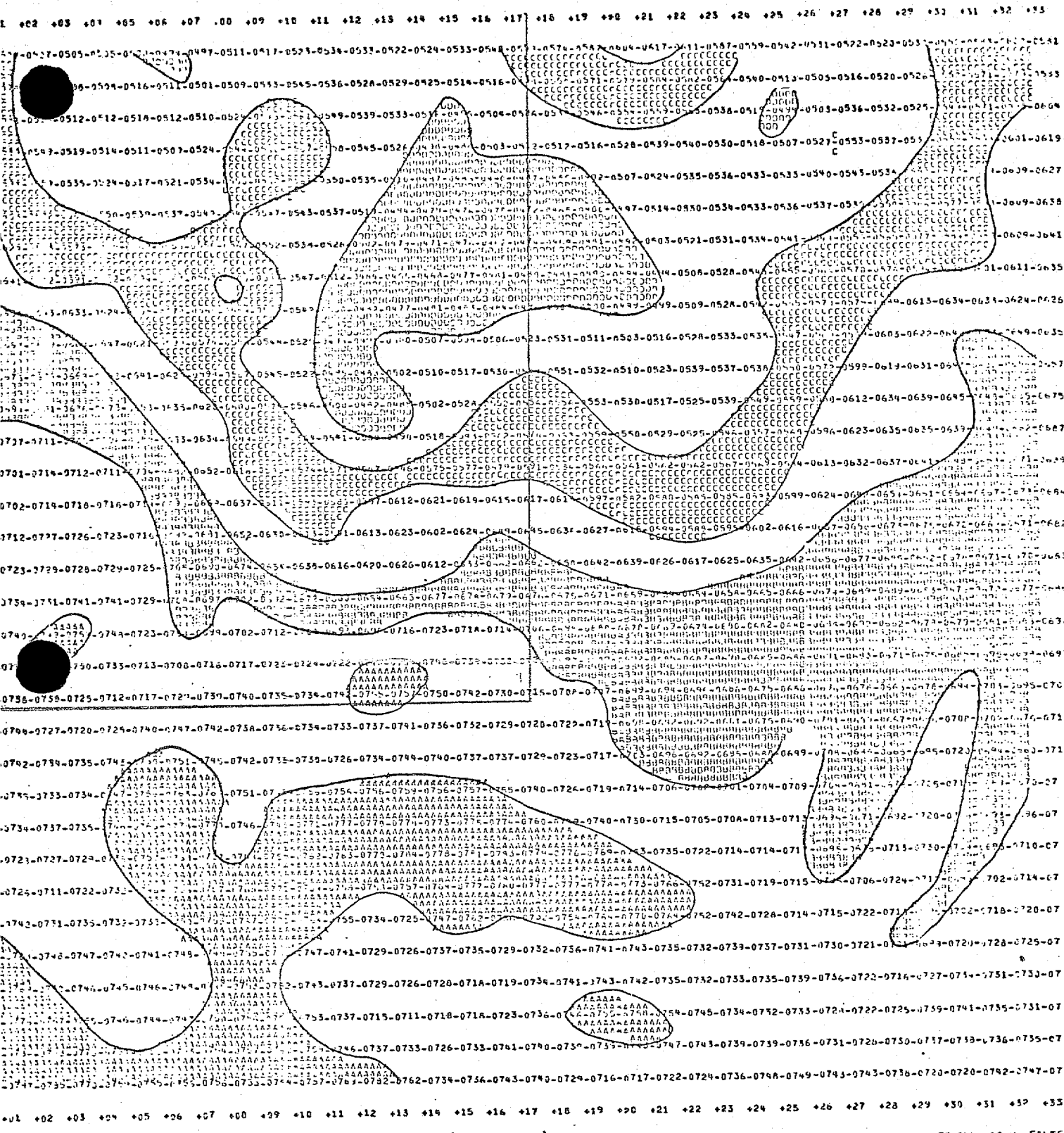
100 MB TEMP DEG CEL +10 H FILTER HALFGRID (Simulates Operational Output)
H
100 MB TEMP DEG CEL +10 H FILTE

figure 5A

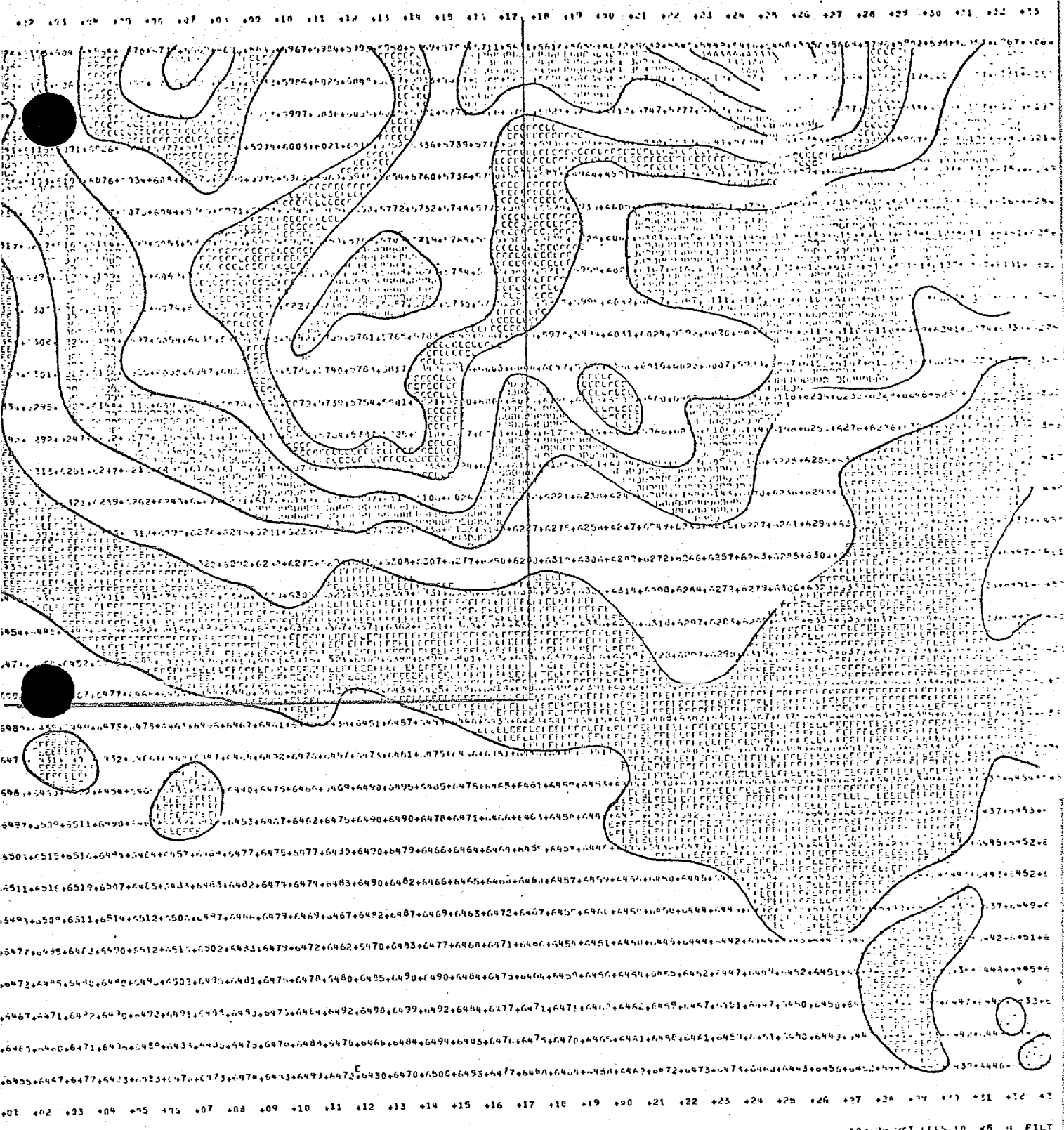

figure 5B

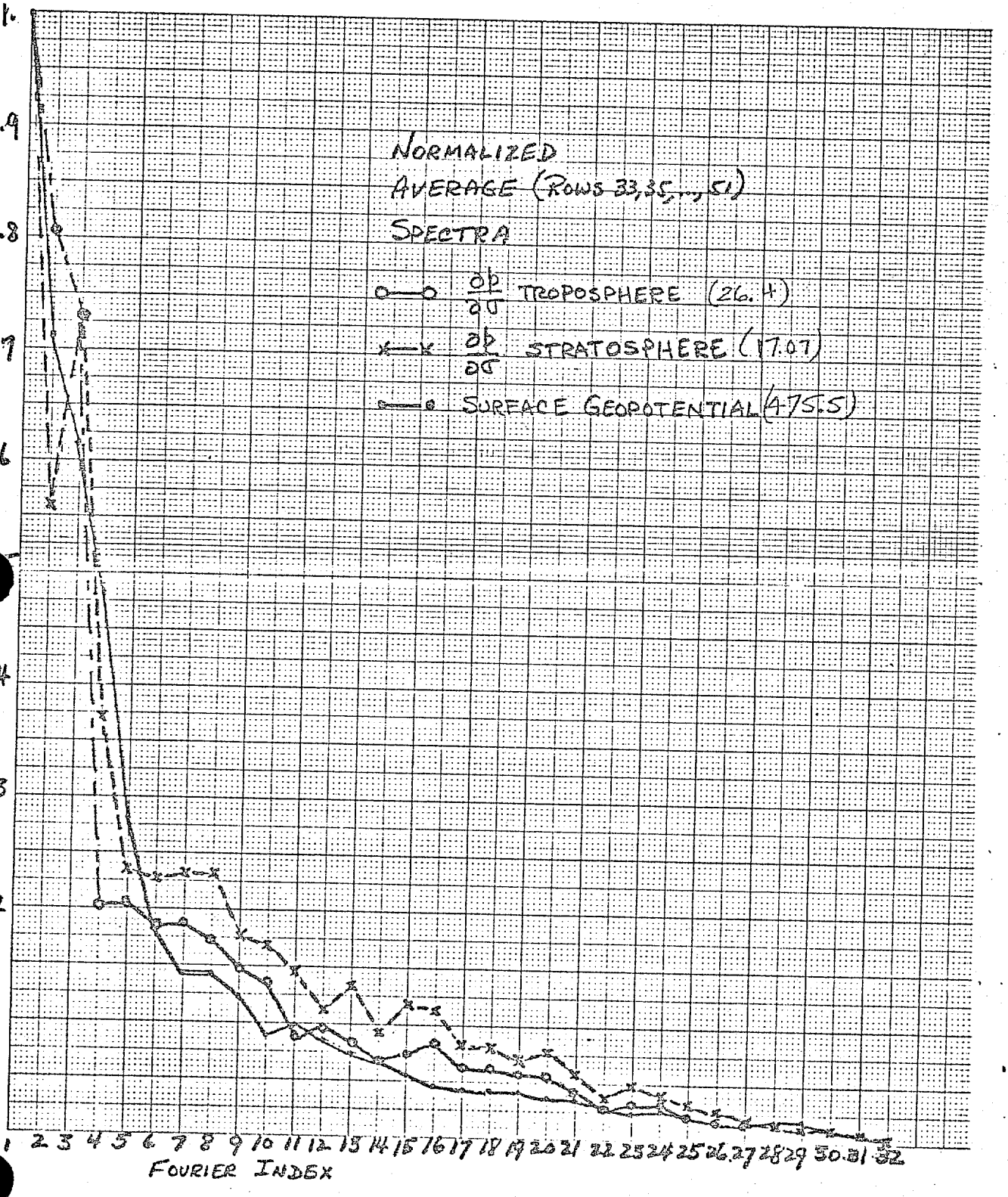
NORMALIZED
AVERAGE (ROWS 33,35,...,51)
SPECTRA
∂p/∂σ TROPOSPHERE (26.4)
∂p/∂σ STRATOSPHERE (17.07)
SURFACE GEOPOTENTIAL (475.5)
AMPLITUDE
FOURIER INDEX
1.
.9
.8
.7
.6
.4
.3
.2
.1
0
1 2 3 4 5 6 7 8 9 10 11 12 13 14 15 16 17 18 19 20 21 22 23 24 25 26 27 28 29 30 31 32

figure 6

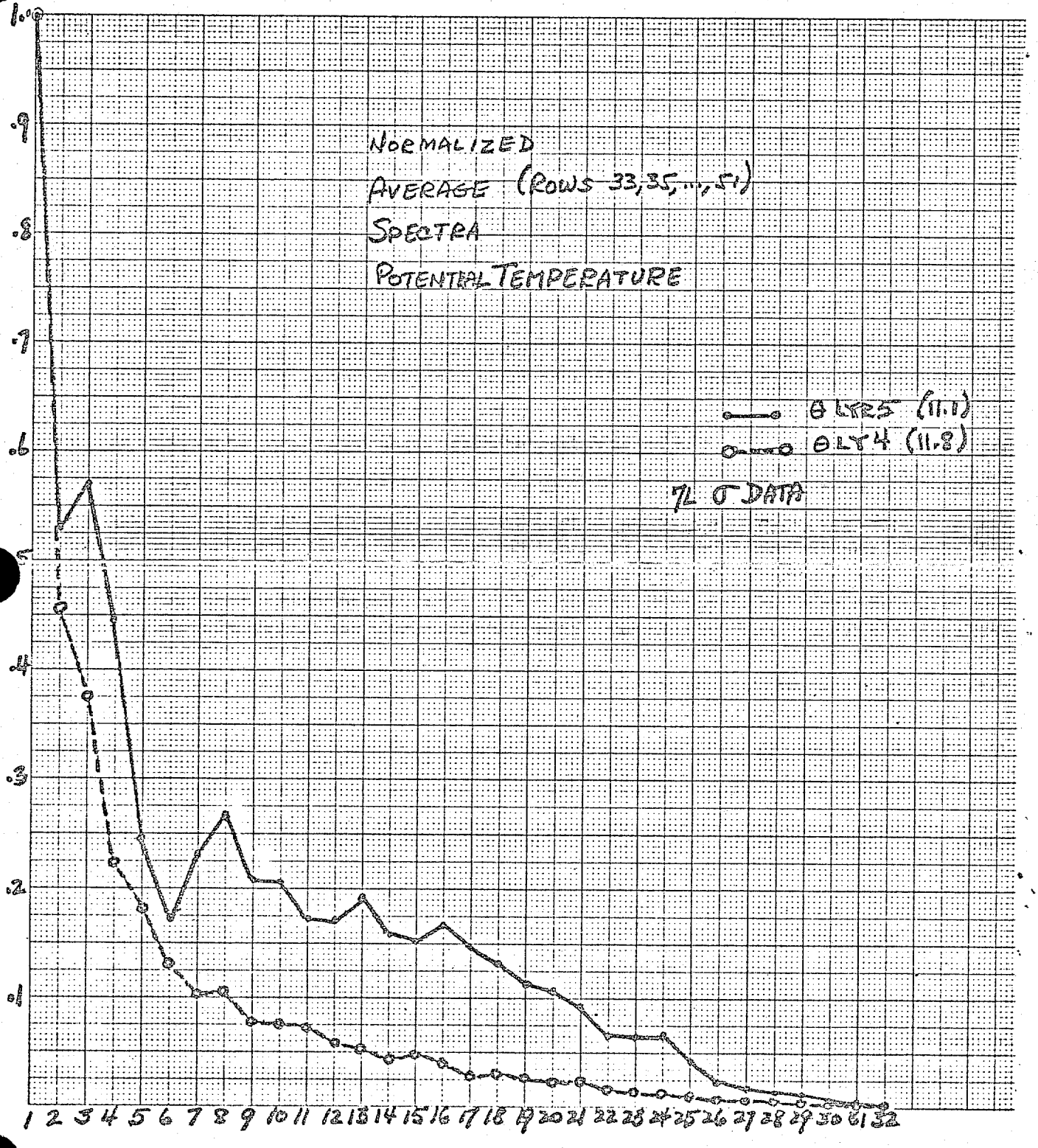

Figure 7

47 1320
K+E 10 X 10 TO ½ INCH • 10 X 15 INCHES
KEUFFEL & ESSER CO. MADE IN U.S.A.

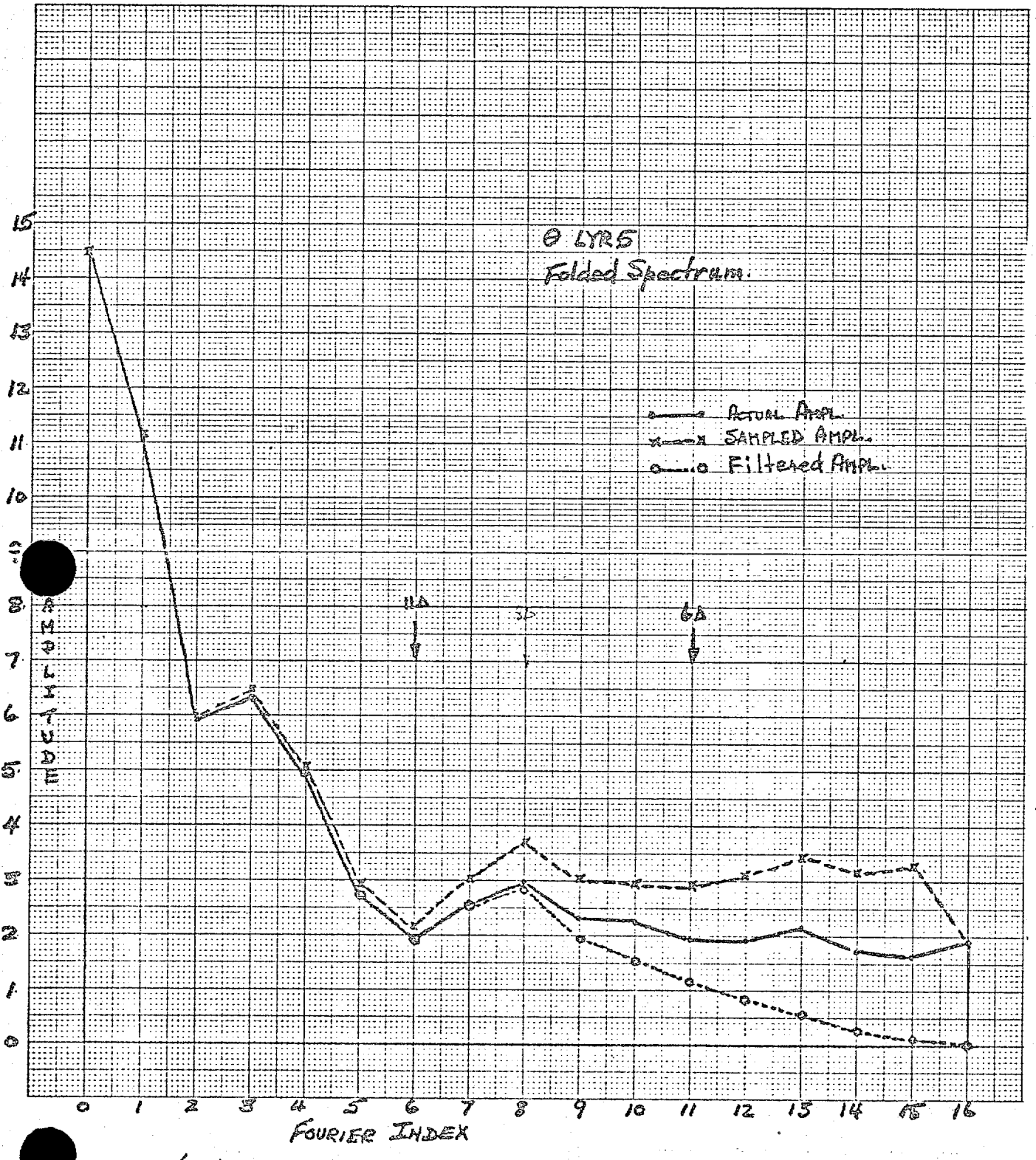
θ LYR 5
Folded Spectrum.
Actual Ampl.
SAMPLED AMPL.
Filtered Ampl.
11Δ
6Δ
AMPLITUDE
FOURIER INDEX
0
1
2
3
4
5
6
7
8
9
10
11
12
13
14
15
16

Figure 8

Figure 9.

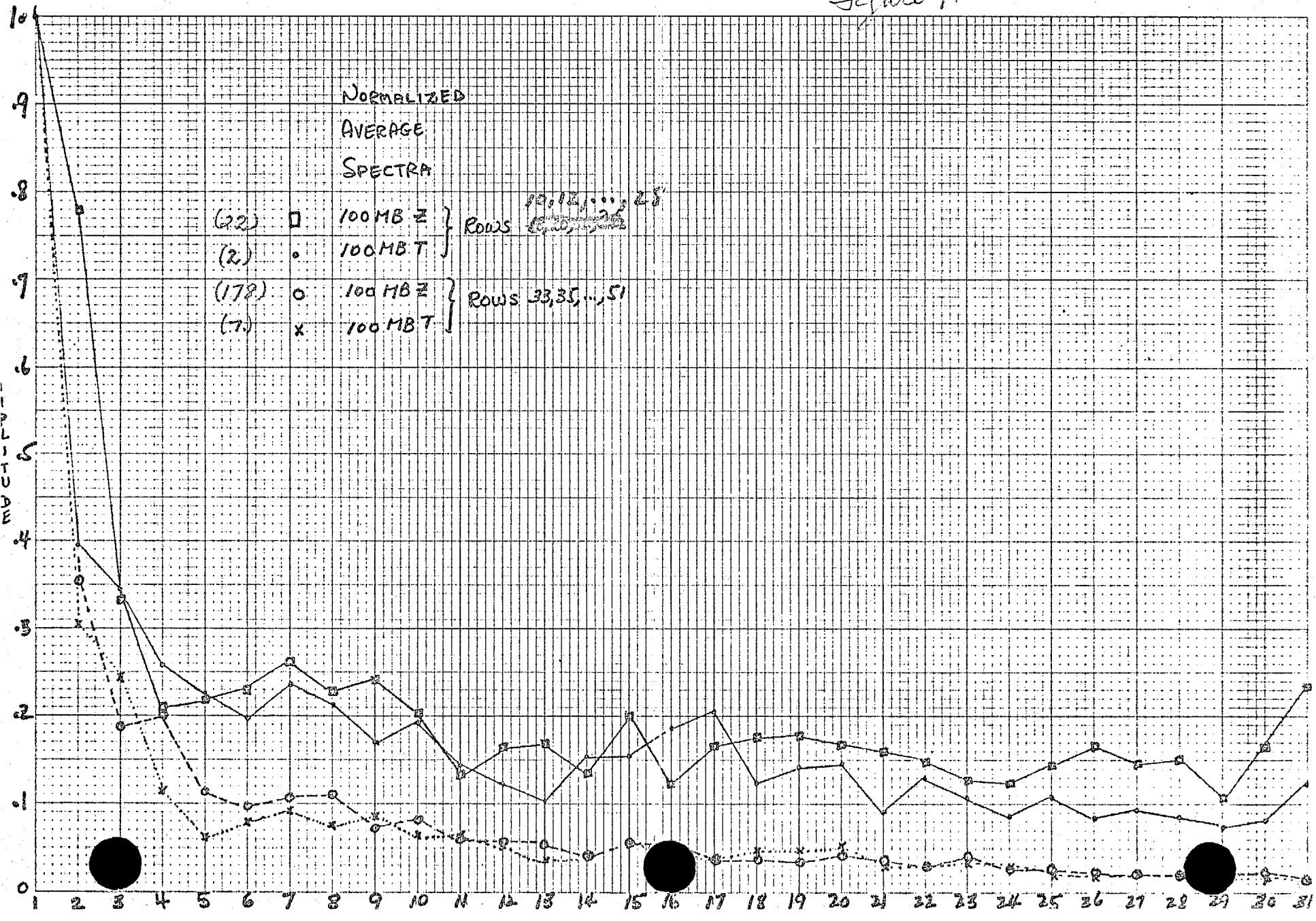
NORMALIZED
AVERAGE
SPECTRA
(22) □ 100 MB Z
(2) • 100 MB T
Rows 19, 21, ..., 25
(178) ○ 100 MB Z
(7) × 100 MB T
Rows 33, 35, ..., 51
AMPLITUDE
1.0
.9
.8
.7
.6
.5
.4
.3
.2
.1
0
1 2 3 4 5 6 7 8 9 10 11 12 13 14 15 16 17 18 19 20 21 22 23 24 25 26 27 28 29 30 31

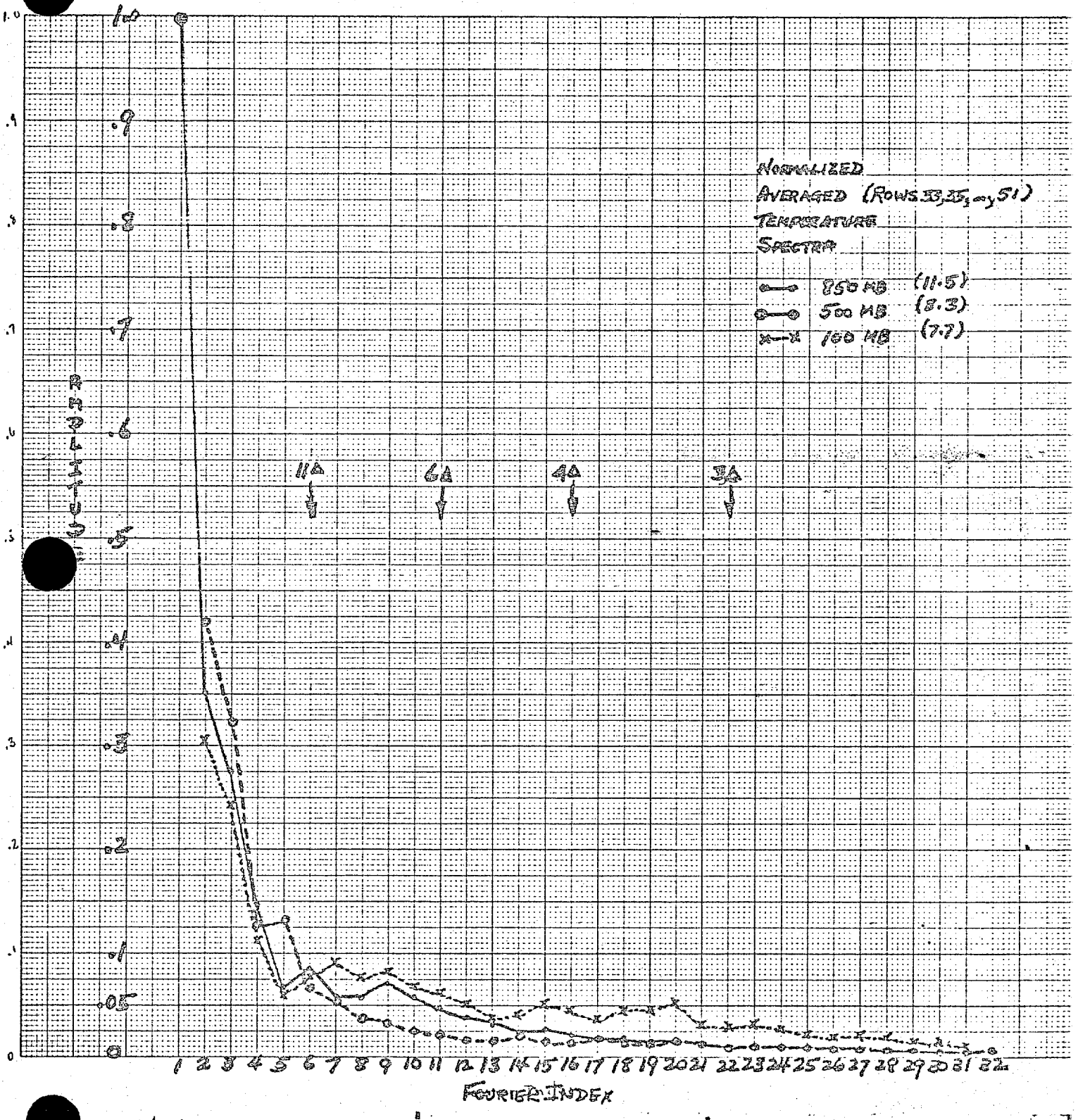
NORMALIZED
AVERAGED (ROWS 33, 35, ..., 51)
TEMPERATURE
SPECTRA
850 MB (11.5)
500 MB (8.3)
100 MB (7.7)
AMPLITUDE
11Δ
6Δ
4Δ
3Δ
FOURIER INDEX

Figure 10

Figure 11

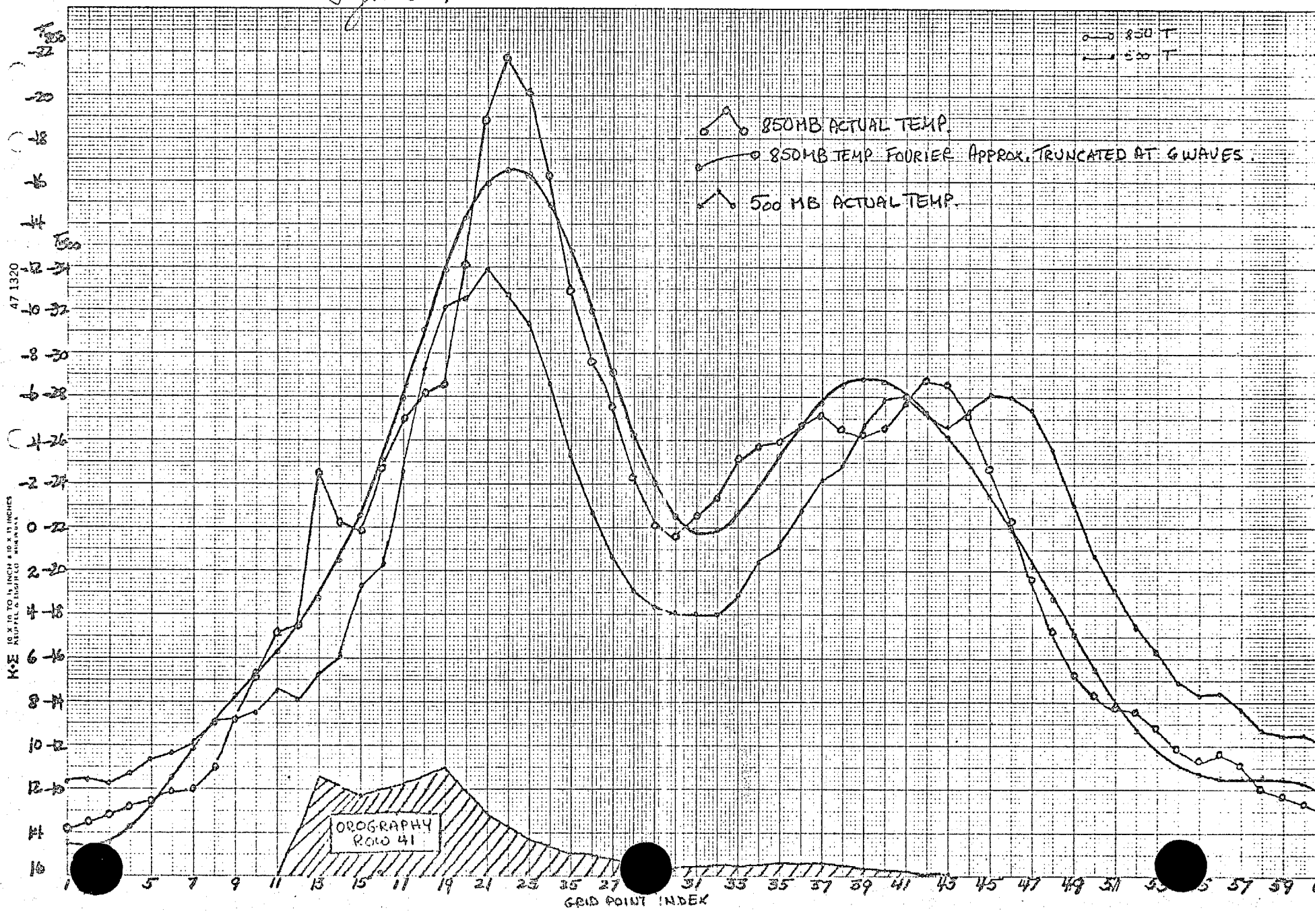
850 T
500 T
850MB ACTUAL TEMP.
850MB TEMP. FOURIER APPROX. TRUNCATED AT 6 WAVES.
500 MB ACTUAL TEMP.
OROGRAPHY
ROW 41
GRID POINT INDEX
K·E
47 1320
10 X 10 TO 1/2 INCH • 10 X 15 INCHES
KEUFFEL & ESSER CO. MADE IN U.S.A.

Figure 12

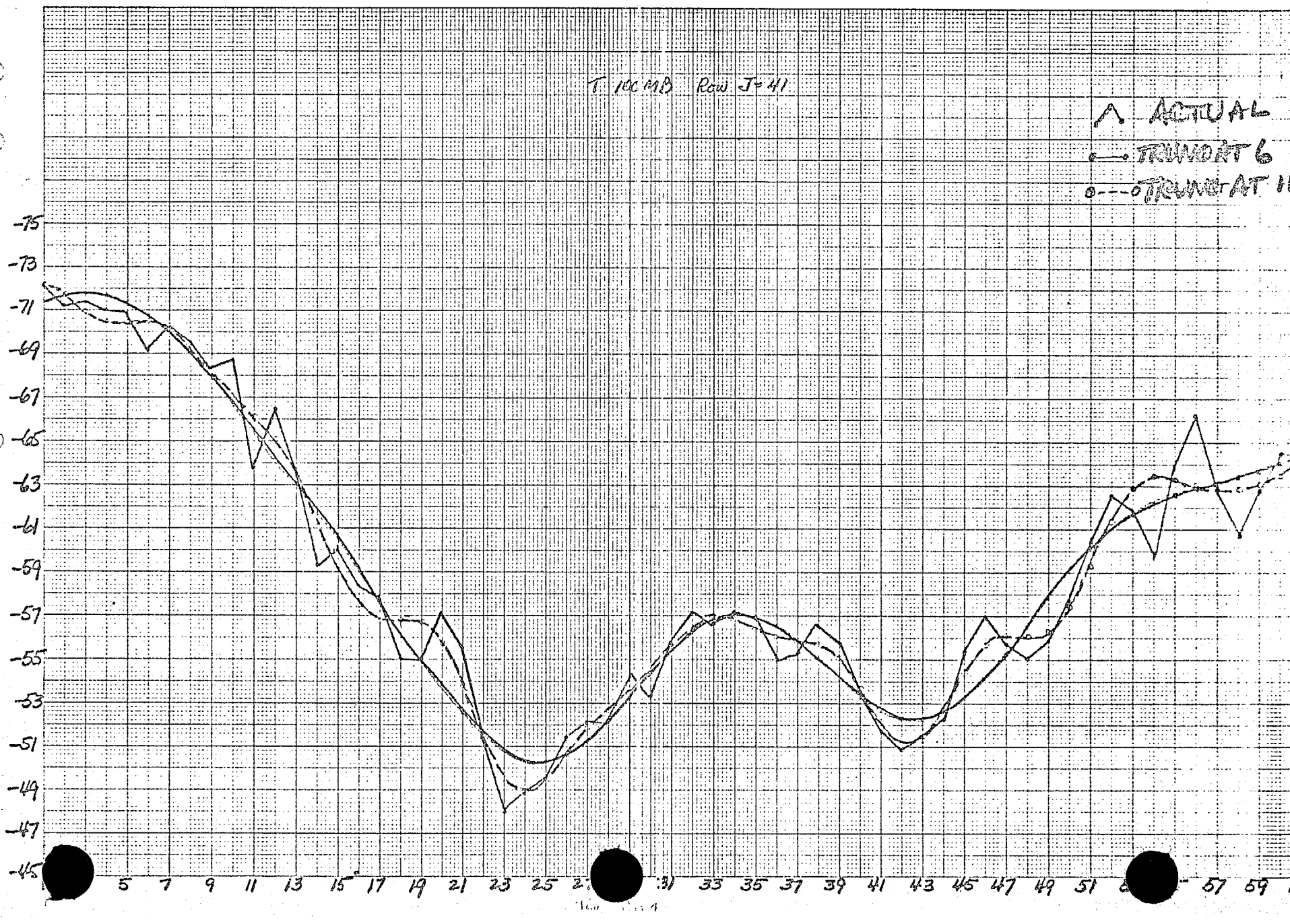
T 100 MB Row J=41
ACTUAL
TRUNCAT 6
TRUNCAT 11
-75
-73
-71
-69
-67
-65
-63
-61
-59
-57
-55
-53
-51
-49
-47
-45
5 7 9 11 13 15 17 19 21 23 25 31 33 35 37 39 41 43 45 47 49 51 57 59
47 1320
K+E 10 X 10 TO ½ INCH • 10 X 10 INCHES KEUFFEL & ESSER CO. MADE IN U.S.A.